

<sup>1</sup> ~~1 Augsburg University, 2211 Riverside Avenue, Minneapolis, MN 55454~~<sup>2</sup> ~~National Ecological Observatory Network, Battelle, 1685 38th Street, Suite 100, Boulder, CO 80301~~<sup>3</sup> ~~Boston University, 5 Cummington Street, Boston, MA 02215~~<sup>4</sup> ~~University of San Francisco, 2130 Fulton Street, San Francisco, CA 94117~~<sup>5</sup> ~~University of Kansas, 1450 Jayhawk Boulevard, Lawrence, KS 66045~~

## <sup>6</sup> **Acknowledgments**

<sup>7</sup> ~~JZ acknowledges Kathleen O'Rourke for code development. NZ thanks technical staff at~~  
<sup>8</sup> ~~USF for support with field gear assembly and shipping. We thank the NEON field staff and~~  
<sup>9</sup> ~~assignable assets teams for facilitating each of the six NEON site visits. We are grateful to~~  
<sup>10</sup> ~~LI-COR technical staff for helpful discussions about optimal soil chamber sampling methods.~~  
<sup>11</sup> ~~This work was supported by NSF DEB grant #2017829 awarded to JZ, and NSF DEB grant~~  
<sup>12</sup> ~~#2017860 awarded to NZ. This material is based in part upon work supported by the National~~  
<sup>13</sup> ~~Ecological Observatory Network (NEON), a program sponsored by the U.S. National Science~~  
<sup>14</sup> ~~Foundation (NSF) and operated under cooperative agreement by Battelle. We also thank the~~  
<sup>15</sup> ~~reviewers and subject editor for their constructive feedback.~~

## <sup>16</sup> **Conflict of Interest Statements**

<sup>17</sup> ~~None of the authors have a financial, personal, or professional conflict of interest related to~~  
<sup>18</sup> ~~this work.~~

## <sup>19</sup> **Author Contributions**

20 Conceptualization: JZ, NZ; Methodology: EA, JZ, NZ; Software: JZ, NZ, ZW, EA, DM, RA,  
21 LX, LL; Validation: JZ, NZ; Formal Analysis: JZ, NZ, DM, RA, LX, LL; Investigation: JZ,  
22 NZ, RF-S, CT, NA-W, LB; Resources: JZ, NZ; Data curation: JZ, NZ, DM, LX; Writing  
23 —original draft: JZ, NZ; Writing —review and editing: JZ, NZ, ZW, EA, CT, DM, LX,;  
24 Visualization: JZ, NZ, DM, RA, LX; Supervision: JZ; NZ; Project Administration: JZ; NZ;  
25 Funding Acquisition: JZ; NZ

## 26 **Data Availability**

27 Anonymous field-collected data, `neonSoilFlux` calculated outputs, and manuscript-generating  
28 code for peer review are provided as supplemental files. An anonymous link for peer review is  
29 here: . This will be made publicly available upon publication.

## 30 **1 Abstract**

- 31 1. Accurate quantification of soil carbon fluxes is essential to reduce uncertainty in estimates  
32 of the terrestrial carbon sink. However, these fluxes vary over time and across ecosystem  
33 types and so it can be difficult to estimate them accurately across large scales. The flux  
34 gradient method estimates soil carbon fluxes using co-located measurements of soil CO<sub>2</sub>  
35 concentration, soil temperature, soil moisture, and other soil properties. The National  
36 Ecological Observatory Network (NEON) provides such data across 20 ecoclimatic domains  
37 spanning the continental U.S., Puerto Rico, Alaska, and Hawai‘i.
- 38 2. We present an R software package (`neonSoilFlux`) that acquires soil environmental data  
39 to compute half-hourly soil carbon fluxes for each soil replicate plot at a given terrestrial

40 NEON site. To assess the computed fluxes, we visited six focal NEON sites and measured  
41 soil carbon fluxes using a closed-dynamic chamber approach.

- 42 3. Outputs from the `neonSoilFlux` showed agreement with measured fluxes ( $R^2$  between  
43 measured and `neonSoilFlux` outputs ranging from ~~0.04 to 0.81~~ 0.12 to 0.77 depending on  
44 calculation method used); measured outputs generally fell within the range of calculated  
45 uncertainties from the gradient method. Calculated fluxes from `neonSoilFlux` aggregated  
46 to the daily scale exhibited expected site-specific seasonal patterns.
- 47 4. While the flux gradient method is broadly effective, its accuracy is highly sensitive  
48 to site-specific inputs, including the extent to which gap-filling techniques are used to  
49 interpolate missing sensor data and to estimates of soil diffusivity and moisture content.  
50 Future refinement and validation of `neonSoilFlux` outputs can contribute to existing  
51 databases of soil carbon flux measurements, providing near real-time estimates of a critical  
52 component of the terrestrial carbon cycle.

53 **1.1 Keywords**

54 Soil carbon, carbon dioxide, flux gradient, carbon cycle, field validation, soil respiration,  
55 ecosystem variability, diffusion

56 **2 Data for peer review**

57 ~~Anonymous field-collected data, `neonSoilFlux` calculated outputs, and manuscript-generating~~  
58 ~~code for peer review are provided as supplemental files. An anonymous link for peer review is~~  
59 ~~here: . This will be made publicly available upon publication.~~

## 60 2 Introduction

61 Soils contain the planet's largest reservoir of terrestrial carbon (Jobbágy & Jackson, 2000). A  
62 critical component of this reservoir is soil organic matter, the accumulation of which is influenced  
63 by biotic factors such as above-ground plant inputs (Jackson et al., 2017). These inputs in  
64 turn are influenced by environmental factors such as growing season length, temperature, and  
65 moisture (Desai et al., 2022), which also affect the breakdown of soil organic matter and its  
66 return to the atmosphere. Across heterogeneous terrestrial landscapes, the interplay between  
67 these biotic and abiotic factors influence the size of the soil contribution to the terrestrial  
68 carbon sink (Friedlingstein et al., 2025). However, the heterogeneity of these processes across  
69 diverse ecosystems in the context of rapid environmental change leads to large uncertainty  
70 about the magnitude of this sink in the future, and thus there remains a pressing need to  
71 quantify changes in soil carbon pools and fluxes across scales.

72 Ecological observation networks such as the United States' National Ecological Observatory  
73 Network (NEON) and others (e.g. the globally-distributed FLUXNET or the European Inte-  
74 grated Carbon Observation System) present a significant advancement in the nearly continuous  
75 observation of biogeochemical processes at the continental scale. Notably, at 47 terrestrial  
76 sites across the continental United States that span 20 ecoclimatic domains, NEON provides  
77 half-hourly measurements of soil CO<sub>2</sub> concentration, temperature, and moisture at different  
78 vertical depths. Each of these NEON sites also encompasses measurements of the cumulative  
79 sum of all ecosystem carbon fluxes in an airshed using the eddy covariance technique (Baldocchi,  
80 2014). Soil observations provided by NEON are on the same timescale and standardized with  
81 eddy covariance measurements from FLUXNET. These types of nearly continuous observational  
82 data (NEON and FLUXNET) can be used to reconcile differences between model-derived  
83 or data-estimated components of ecosystem carbon flux (Jian et al., 2022; Luo et al., 2011;  
84 Phillips et al., 2017; J. Shao et al., 2015; P. Shao et al., 2013; Sihi et al., 2016).

85 Estimated or observed soil carbon fluxes are a key metric for understanding change in soil  
86 carbon pools over time (Bond-Lamberty et al., 2024). A soil carbon flux to the atmosphere ( $F_S$ ,  
87 units  $\mu\text{mol m}^{-2} \text{s}^{-1}$ ), represents the aggregate process of transfer of soil  $\text{CO}_2$  to the atmosphere  
88 from physical and biological processes (e.g. diffusion and respiration). Soil carbon fluxes can  
89 be assumed to encompass soil carbon respiration from autotrophic or heterotrophic sources  
90 (Davidson et al., 2006) and modeled with a exponential  $Q_{10}$  paradigm (Bond-Lamberty et al.,  
91 2004; Chen & Tian, 2005; Hamdi et al., 2013).

92 One common method by which  $F_S$  is measured in the field is through the use of soil chambers  
93 in a closed, well-mixed system (Norman et al., 1997) with headspace trace gas concentrations  
94 measured with an infrared gas analyzer (IRGA).  $F_S$  can also be estimated from soil  $\text{CO}_2$   
95 measurements at different depths in the soil using the flux-gradient method (Maier & Schack-  
96 Kirchner, 2014). Closed-chamber IRGA measurements, while being the most common method,  
97 require either frequent in-person site visits or expensive and fragile automated systems. The  
98 potential of the gradient method is that fluxes can be estimated from continuous data recorded  
99 by robust solid-state sensors. The flux-gradient method is an approach that uses conservation of  
100 mass to calculate flux at a vertical soil depth  $z$  at steady state by applying Fick's law of diffusion.  
101 A simplifying assumption for the flux-gradient method is that there is no mass transfer in the  
102 other spatial dimensions  $x$  and  $y$  (Maier & Schack-Kirchner, 2014). The diffusivity profile, a  
103 key component of this calculation, varies across the soil depth as a function of soil temperature,  
104 soil volumetric water content, atmospheric air pressure, and soil bulk density (Millington &  
105 Shearer, 1971; Moldrup et al., 1999; Sallam et al., 1984).

106 Databases such as the Soil Respiration Database (SRDB) or the Continuous Soil Respiration  
107 Database (COSORE) add to the growing network of resources for making collected observations  
108 of soil fluxes available to other researchers (Bond-Lamberty, 2018; Bond-Lamberty et al., 2020;  
109 Bond-Lamberty & Thomson, 2010; Jian et al., 2021; Jiang et al., 2024). However, these

110 databases currently encompass primarily direct soil measurements of fluxes (i.e. those using  
111 methods like the closed-chamber method described above). Currently, NEON provides all  
112 measurements to calculate  $F_S$  from Fick's law, but soil flux as a derived data product was  
113 descoped from the initial network launch due to budget constraints (Berenbaum et al., 2015).  
114 Deriving estimates of  $F_S$  using continuous sensor data across NEON sites using NEON data  
115 thus remains a high priority.

116 This study describes an R software package, `neonSoilFlux`, that computes a standardized  
117 estimate of  $F_S$  at all terrestrial NEON sites using the flux-gradient method. Using direct  
118 chamber-based field observations of soil carbon dioxide flux from a subset of terrestrial NEON  
119 sites spanning six states, we provide a direct validation of  $F_S$  from `neonSoilFlux`. While  
120 open source R software tools currently exist for processing chamber-based flux measurements  
121 (Jurasinski et al., 2022; Pedersen, 2024; Rheault et al., 2024; Wilson et al., 2024; Zhao, 2019),  
122 to our knowledge this is the first package that incorporates NEON data directly.

123 Key objectives of this study are to:

- 124 1. Apply the flux-gradient method to estimate soil CO<sub>2</sub> flux from continuous sensor mea-  
125 surements across six NEON sites.
- 126 2. Benchmark estimated soil carbon fluxes against field measurements (e.g. direct chamber  
127 measurements of soil flux).
- 128 3. Identify sources of error in the flux-gradient approach across diverse sites in order to  
129 guide future work.

<sup>130</sup> **3 Materials and Methods**

<sup>131</sup> **3.1 Field methods**

<sup>132</sup> **3.1.1 Focal NEON Sites**

<sup>133</sup> In order to acquire field data to validate model predictions of flux, we selected six terrestrial  
<sup>134</sup> NEON sites for analysis. We conducted roughly week-long field measurement campaigns at  
<sup>135</sup> these sites, which span a range of environmental gradients and terrestrial domains (Table 1).  
<sup>136</sup> SJER, SRER, and WREF were visited during May and June of 2022, and WOOD, KONZ, and  
<sup>137</sup> UNDE during May and June of 2024. Permits or waivers were sought and approved prior to  
<sup>138</sup> field work at all six sites. In 2022, research activities were conducted whole or in part on the  
<sup>139</sup> Wind River Experimental Forest within the Gifford Pinchot National Forest. No permit was  
<sup>140</sup> required for this work. Approval for research at San Joaquin Experimental Range was granted  
<sup>141</sup> by Dr. Angela White in May 2022 and for research at Santa Rita Experimental Range by  
<sup>142</sup> Dr. Mitch McClaran in May 2022. In 2024, permits were received for work at WOOD (Chase  
<sup>143</sup> Lake WMD; permit number 62515-24-020), KONZ (Konza Prairie Biological Station; permit  
<sup>144</sup> number 766), and UNDE (University of Notre Dame Environmental Research Center; permit  
<sup>145</sup> number UNDERC-2024-5).

<sup>146</sup> **3.1.2 Soil collar placement**

<sup>147</sup> Either one (2022 sampling campaign) or two (2024 sampling campaign) PVC soil collars (20.1  
<sup>148</sup> cm inside diameter) were installed in close proximity to the permanent NEON soil sensors at  
<sup>149</sup> each site (Figure 1). As instruments in the NEON soil sensor arrays can occasionally break  
<sup>150</sup> down or stop working, the specific soil plot where we made measurements was chosen at each  
<sup>151</sup> site in consultation with NEON staff to maximize likelihood of quality soil sensor measurements

152 during the duration of the IRGA measurements. The plot selected at each site (out of the 5 in  
153 each replicate array at each site) are presented in the last column of Table 1. After installation,  
154 collar(s) were left to equilibrate for approximately 24 hours prior to any measurements being  
155 taken.

156 **3.1.3 Infrared gas analyzer measurements of soil CO<sub>2</sub> flux**

157 In 2022, we then made measurements of flux on an hourly interval for 8 hours each day.  
158 Measurements were taken from roughly 8 am to 4 pm, with the time interval selected to  
159 capture the majority of the diurnal gradient of soil temperature each day. These measurements  
160 were made using a LI-6800 infrared gas analyzer instrument (LI-COR Environmental, Lincoln,  
161 NE) fitted with a soil chamber attachment (attachment 6800-09). In 2024, we again used the  
162 same LI-6800 instrument, but made half-hourly measurements over an approximately 8 hour  
163 period. In addition, in 2024 we also installed a second collar and used a second instrument, an  
164 LI-870 CO<sub>2</sub> IRGA, connected to an automated robotic chamber (LI-COR chamber 8200-104)  
165 controlled by an LI-8250 multiplexer to make automated measurements. The multiplexer was  
166 configured to take half-hourly measurements 24 hours a day for the duration of our sampling  
167 bout at each site. Each instrument was paired with a soil temperature and moisture probe  
168 (Stevens HydraProbe, Stevens Water, Portland, OR) that was used to make soil temperature  
169 and moisture measurements concurrent with the CO<sub>2</sub> flux measurements. Chamber volumes  
170 were set by measuring collar offsets at each site. System checks were conducted daily for the  
171 LI-6800 and weekly for the LI-8250. Instruments were factory calibrated before each field  
172 season.

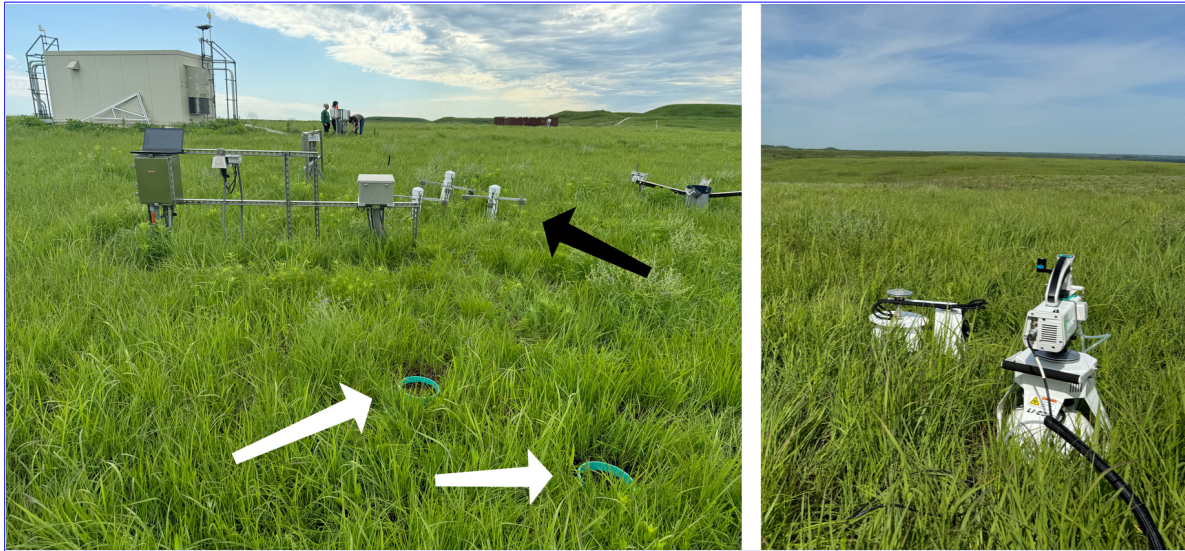


Figure 1: Spatial layout of field sampling using a closed-dynamic chamber setup at a representative NEON site (KONZ). Left image shows collars (white arrows) and permanent soil sensor installation (black arrow) and right image shows the LI-6800 (foreground) and LI-8200-104 (background) instruments placed on the collars.

g of NEON sites studied for field work and analysis. Site refers to NEON site : Santa Rita Experimental Range (SRER), San Joaquin Experimental Range (SJER), Wind River Experimental Forest (WREF), Chase Lake National Wildlife Refuge (WOOD), Konza Prairie Biological Station (KONZ), and the University of Notre Dame Environmental Research Center (UNDE). Location is reported in decimal degrees of latitude and longitude. Other abbreviations include Mean Annual Temperature (MAT);  $\bar{T}_S$ : average soil temperature during field measurements;  $\overline{SWC}$ : average soil water content during field measurements. Dates refer to field measurement dates for each site. Plot refers to the particular location in the soil sensor array (labeled as HOR by NEON) where field measurements were made.

Site	Location	Ecosystem	MAT	$\bar{T}_S$	MAP	$\overline{SWC}$	Dates	Plot
SRER	31.91068, -110.83549	Shrubland	19.3 °C	47.6 °C	346 mm	4.0%	May 29– June 1 2022	004
SJER	37.10878, -119.73228	Oak woodland	16.4 °C	41.7 °C	540 mm	1.2%	June 1–4 2022	005
WREF	45.82049, -121.95191	Evergreen forest	9.2 °C	15.3 °C	2225 mm	27.2%	June 7–9 2022	001
WOOD	47.1282, -99.241334	Restored prairie	4.9 °C	14.9 °C	495 mm	14.9%	June 3–9 2024	001
KONZ	39.100774, -96.563075	Tallgrass prairie	12.4 °C	23.4 °C	870 mm	23.4%	May 29– June 1 2024	001

g of NEON sites studied for field work and analysis. Site refers to NEON site : Santa Rita Experimental Range (SRER), San Joaquin Experimental Range R), Wind River Experimental Forest (WREF), Chase Lake National Wildlife e (WOOD), Konza Prairie Biological Station (KONZ), and the University tre Dame Environmental Research Center (UNDE). Location is reported in al degrees of latitude and longitude. Other abbreviations include Mean Annual erature (MAT);  $\overline{T_S}$ : average soil temperature during field measurements;  $\overline{SWC}$ : age soil water content during field measurements. Dates refer to field measurement for each site. Plot refers to the particular location in the soil sensor array ed as HOR by NEON) where field measurements were made.

Site	Location	Ecosystem	MAT	$\overline{T_S}$	MAP	$\overline{SWC}$	Dates	Plot
UNDE	46.23391, -89.537254	Deciduous forest	4.3 °C	13.0 °C	802 mm	13.0%	May 22–25 2024	004

### 173 3.1.4 Post-collection processing of field data

174 We used LI-COR SoilFluxPro software (v 5.3.1) to assess the data after collection and to  
 175 inform sampling parameters. We checked appropriateness of dead band and measurement  
 176 durations using built-in evaluation tools. Based on this, the deadband period was set for 30-40  
 177 seconds, depending on the site, and the measurement duration was 180 seconds with a 30  
 178 second pre-purge and a 30 second post-purge at most sites, and a 90 second pre- and post-purge  
 179 at sites with higher humidity due to recent precipitation events. We also assessed the  $R^2$  of  
 180 linear and exponential model fits to measured CO<sub>2</sub> to verify measurement quality.

### 181 3.2 neonSoilFlux R package

182 We developed an R package called `neonSoilFlux` (Zobitz et al., 2024) to compute half-hourly  
 183 soil carbon fluxes and uncertainties from NEON data. The objective of the `neonSoilFlux`  
 184 package is a unified workflow (Figure 2) for soil data acquisition and analysis that supplements  
 185 the existing `neonUtilities` data acquisition R package (Lunch et al., 2025).

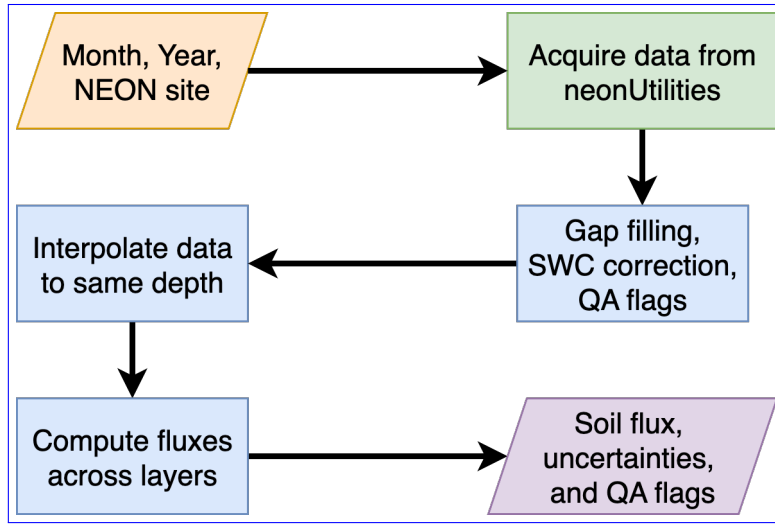


Figure 2: Diagram of `neonSoilFlux` R package. For a given month, year, and NEON site (orange parallelogram), the package acquires all relevant data to compute  $F_S$  using the `neonUtilities` R package (green rectangle). Data are gap-filled according to reported QA flags and adjusted for changes in soil water content (SWC) calibration coefficients, then interpolated to the same measurement depth before computing the soil flux, uncertainties, and final QA flags (blue rectangles). The package reports the associated soil flux, uncertainties, and quality assurance (QA) flags for the user (purple parallelogram).

186 At a given NEON site there are five replicate soil plots, each with measurements of soil  
 187 CO<sub>2</sub> concentration, soil temperature, and soil moisture at different depths (Figure 3).  
 188 The `neonSoilFlux` package acquires measured soil CO<sub>2</sub> concentration ([National Ecological Observatory Network \(NEON\) NEON](#), 2024b), soil temperature ([National Ecological Observatory Network \(NEON\) NEON](#), 2024d), soil water content ([National Ecological Observatory Network \(NEON\) NEON](#), 2024e), barometric pressure from the nearby tower ([National Ecological Observatory Network \(NEON\) NEON](#), 2024a), and soil properties (e.g. bulk density) ([National Ecological Observatory Network \(NEON\) NEON](#), 2024c) from a range of different NEON data products. The static soil properties were collected by NEON staff from a nearby soil pit during initial site characterization and are assumed to be constant at each site. A soil flux calculation is computed at each replicate soil plot.  
 196

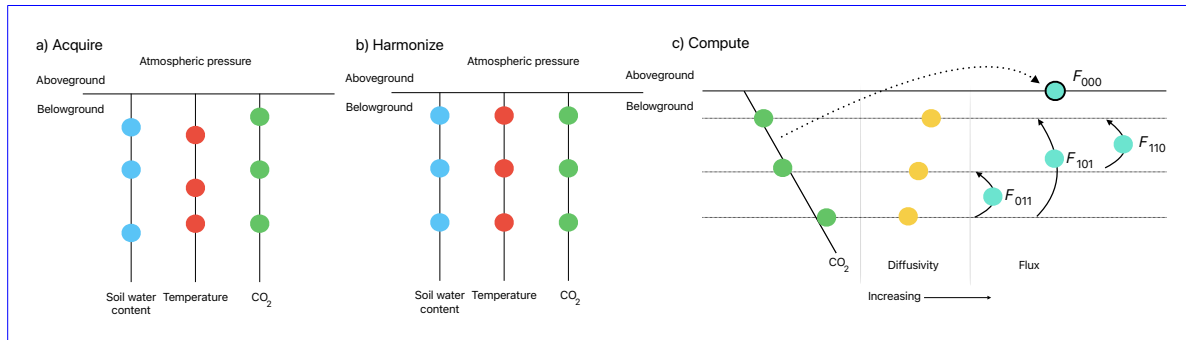


Figure 3: Model diagram of the data workflow for the `neonSoilFlux` R package. a) Acquire: Data are obtained for a given NEON location and horizontal sensor location, which includes soil water content, soil temperature, CO<sub>2</sub> concentration, and atmospheric pressure. All data are screened for quality assurance; if gap-filling of missing data occurs, it is flagged for the user. b) Harmonize: Any belowground data are then harmonized to the same depth as CO<sub>2</sub> concentrations using linear regression. c) Compute: The flux across a given depth is computed via Fick's law, denoted with  $F_{ijk}$ , where  $i$ ,  $j$ , or  $k$  are either 0 or 1 denoting the layers the flux is computed across ( $i =$  closest to surface,  $k =$  deepest).  $F_{000}$  represents a flux estimate where the gradient  $dC/dz$  is the slope of a linear regression of CO<sub>2</sub> with depth.

197 The workflow to compute a value of  $F_S$  with `neonSoilFlux` consists of three primary steps,  
 198 illustrated in Figure 3. First, NEON data are acquired for a given site and month via the

199 `neonUtilities` R package (yellow parallelogram and green rectangle in Figure 2 and Panel  
200 a in Figure 3). Acquired environmental data can be exported to a comma separated value  
201 file for additional analysis. Quality assurance (QA) flags are reported as an indicator variable.  
202 Since the calibration coefficients on the soil water content sensors have changed over time  
203 ([National Ecological Observatory Network \(NEON\)](#)[NEON](#), 2024e), raw sensor measurements  
204 were back-calculated and soil-specific calibrations were applied following Ayres et al. (2024) to  
205 generate a consistent time series at each measurement location.

206 The second step is harmonizing the data to compute soil fluxes across soil layers. This  
207 step consists of three different actions (blue rectangles in Figure 2 and Panel b in Figure 3).  
208 If a given observation by NEON is reported as not passing a quality assurance check, we  
209 applied a gap filling method to replace that measurement with its monthly mean at that same  
210 depth (Section 3.2.1). Belowground measurements of soil water and soil temperature are then  
211 interpolated to the same depth as soil CO<sub>2</sub> measurements. The diffusivity (Section 3.2.2) and  
212 soil flux across different soil layers (Section 3.2.3) are then computed.

213 The third and final step is computing a surface soil flux through extrapolation to the surface  
214 (purple parallelogram in Figure 2 and Panel c in Figure 3). Uncertainty on a soil flux  
215 measurement is computed through quadrature. An aggregate quality assurance (QA) flag for  
216 each environmental measurement is also reported, representing if any gap-filled measurements  
217 were used in the computation of a soil flux. Within the soil flux-gradient method, several  
218 different approaches can be used to derive a surface flux (Maier & Schack-Kirchner, 2014); the  
219 `neonSoilFlux` package reports four different possible values for soil surface flux (Section 3.2.3)  
220 for each of two different methods of diffusivity estimation, for a total of eight estimates of  
221 flux.

222 **3.2.1 Gap-filling routine**

223 NEON reports QA flags as binary values for each measurement and half-hourly interval. For a  
224 given half-hour, if any input variable (soil CO<sub>2</sub> concentration, soil temperature, or soil moisture)  
225 at depth  $z$  is flagged, computation of  $F_S$  is not possible. To address this, flagged measurements  
226 and their uncertainties were replaced with a bootstrapped monthly mean ( $\bar{m}$ ) and monthly  
227 standard deviation ( $\bar{s}$ ) (Efron & Tibshirani, 1994).

228 For each month, depth  $z$ , and variable, we computed bootstrapped estimates of  $\bar{m}$  and  $\bar{s}$   
229 from the vectors of unflagged measurements (**m**), reported standard errors ( $\sigma$ ), and the 95%  
230 confidence interval ( $\epsilon$ , or expanded uncertainty; Farrance & Frenkel (2012)). We also defined a  
231 bias vector  $\mathbf{b} = \sqrt{\epsilon^2 - \sigma^2}$ , which quantifies the spread of uncertainty in a given period and is  
232 incorporated into  $\bar{m}$ .

233 From these, 5000 bootstrap samples were generated for **m**,  $\sigma$ , and **b**. For each sample  
234 ( $m_k, b_k, \sigma_k$ ), we generated a vector **n** (length  $N = 5000$ ) by drawing from a normal distribution  
235 with mean  $m_k + b_k$  and standard deviation  $\sigma_k$ . The sample mean and standard deviation were  
236 then computed from **n**. The resulting distributions of sample means and sample standard  
237 deviations provided the bootstrapped monthly mean ( $\bar{m}$ ) and standard error ( $\bar{s}$ ) respectively.

238 This gap-filling procedure provides a consistent treatment across all data streams. However,  
239 alternative approaches may be better suited for longer gaps (e.g., correlations with other NEON  
240 measurement levels or soil plots) or for variable-specific conditions. We discuss the effect of  
241 gap-filling on our results in Section 5.1.

<sup>242</sup> **3.2.2 Soil diffusivity**

<sup>243</sup> Soil diffusivity  $D_a$  at a given measurement depth is the product of the diffusivity in free air  
<sup>244</sup>  $D_{a,0}$  ( $\text{m}^2 \text{ s}^{-1}$ ) and the tortuosity  $\xi$  (no units) (Millington & Shearer, 1971).

<sup>245</sup> We compute  $D_{a,0}$  with Equation 1:

$$D_{a,0} = 0.0000147 \cdot \left( \frac{T_i + 273.15}{293.15} \right)^{1.75} \cdot \left( \frac{P}{101.3} \right) \quad (1)$$

<sup>246</sup> where  $T_i$  is soil temperature ( $^\circ\text{C}$ ) at depth  $i$  (National Ecological Observatory Network  
<sup>247</sup> (NEON) (NEON), 2024d) and  $P$  surface barometric pressure (kPa) (National Ecological  
<sup>248</sup> Observatory Network (NEON) (NEON), 2024a).

<sup>249</sup> Previous studies by Sallam et al. (1984) and Tang et al. (2003) demonstrated the sensitivity  
<sup>250</sup> of modeled  $F_S$  depending on the tortuosity model ( $\xi$ ) used to compute diffusivity. At low  
<sup>251</sup> soil water content, the choice of tortuosity model can lead to order-of-magnitude differences  
<sup>252</sup> in  $D_a$ , which in turn affect modeled  $F_S$ . The neonSoilFlux package currently includes two  
<sup>253</sup> approaches to calculate  $\xi$ , representing the range of tortuosity behavior reported in Sallam et  
<sup>254</sup> al. (1984).

<sup>255</sup> The first approach is the Millington-Quirk model (Millington & Shearer, 1971), in which  
<sup>256</sup> tortuosity depends on both porosity and soil water content:

$$\xi = \frac{(\phi - SWC_i)^{10/3}}{\phi^2} \quad (2)$$

257 In Equation 2,  $SWC$  is the soil water content at depth  $i$  ([National Ecological Observatory](#)  
 258 [Network \(NEON\)](#)[NEON](#), 2024e) and  $\phi$  is the porosity, which in turn is a function of soil  
 259 physical properties ([National Ecological Observatory Network \(NEON\)](#)[NEON](#), 2024c):

$$\phi = \left(1 - \frac{\rho_s}{\rho_m}\right) (1 - f_V) \quad (3)$$

260 In Equation 3,  $\rho_m$  is the particle density of mineral soil ( $2.65 \text{ g cm}^{-3}$ ),  $\rho_s$  the soil bulk density ( $\text{g}$   
 261  $\text{cm}^{-3}$ ) excluding coarse fragments greater than 2 mm ([National Ecological Observatory Network](#)  
 262 [\(NEON\)](#)[NEON](#), 2024c), and  $f_V$  is a site-specific value that accounts for the proportion of  
 263 soil fragments between 2-20 mm. Soil fragments greater than 20 mm were not estimated due  
 264 to limitations in the amount of soil that can be analyzed ([National Ecological Observatory](#)  
 265 [Network \(NEON\)](#)[NEON](#), 2024c). We assume that rock fragments contain no internal pores.

266 The Millington-Quirk model assumes  $\xi$  is modulated by the amount of fluid saturation in soil  
 267 pores (Millington & Shearer, 1971). In contrast, the Marshall model (Marshall, 1959) expresses  
 268 tortuosity as only a function of porosity ( $\xi = \phi^{1.5}$ ), with  $\phi$  defined from Equation 3. The  
 269 Marshall model is independent of soil water content and assumes tortuosity is only governed  
 270 by soil structure. The `neonSoilFlux` package allows users to choose the tortuosity model most  
 271 appropriate for site-specific conditions and research goals.

### 272 3.2.3 Soil flux computation

273 We applied Fick's law (Equation 4) to compute the soil flux  $F_{ij}$  ( $\mu\text{mol m}^{-2} \text{ s}^{-1}$ ) across two  
 274 soil depths  $i$  and  $j$ :

$$F_{ij} = -D_a \frac{dC}{dz} \quad (4)$$

275 where  $D_a$  is the diffusivity ( $\text{m}^2 \text{ s}^{-1}$ ) and  $\frac{dC}{dz}$  is the gradient of  $\text{CO}_2$  molar concentration ( $\mu\text{mol m}^{-3}$ , so the gradient has units of  $\mu\text{mol m}^{-3} \text{ m}^{-1}$ ). The soil surface flux is theoretically defined  
276 by applying Equation 4 to measurements collected at the soil surface and directly below the  
277 surface. Measurements of soil temperature, soil water content, and soil  $\text{CO}_2$  molar concentration  
278 across the soil profile allow for application of Equation 4 across different soil depths. Each  
279 site had three measurement layers, so we denote the flux as a three-digit subscript  $F_{ijk}$  with  
280 indicator variables  $i$ ,  $j$ , and  $k$  indicate if a given layer was used (written in order of increasing  
281 depth), according to the following:

- 283 •  $F_{000}$  is a surface flux estimate using the intercept of the linear regression of  $D_a$  with  
284 depth and the slope from the linear regression of  $\text{CO}_2$  with depth (which represents  $\frac{dC}{dz}$   
285 in Fick's Law). Tang et al. (2003) used this approach to compute fluxes in an oak-grass  
286 savannah.
- 287 •  $F_{110}$  is a flux estimate across the two shallowest measurement layers.
- 288 •  $F_{011}$  is a flux estimate across the two deepest measurement layers.
- 289 •  $F_{101}$  is a flux estimate across the shallowest and deepest measurement layers.

290 For  $F_{110}$ ,  $F_{011}$ , and  $F_{101}$ , the diffusivity used in Fick's Law is always at the deeper measurement  
291 layer. When used as a surface flux estimate we assume  $\text{CO}_2$  remains constant above this flux  
292 depth. Uncertainty in all  $F_{ijk}$  values was quantified using quadrature (Taylor, 2022). These  
293 computed fluxes could provide the basis for additional soil flux estimates. For example, Tang et  
294 al. (2005) estimated surface flux by linearly extrapolating  $F_{110}$  and  $F_{011}$  to the soil surface.

### 295 3.3 Post processing evaluation

296 Following collection of field measurements and calculation of the soil fluxes from `neonSoilFlux`  
297 package, we compared measured  $F_S$  based on closed-dynamic chamber measurements with the

Table 2: Summary of measured soil characteristics and flux results from field measurements across six NEON sites using a LI-COR 6800 (LI-870/8250 measurements omitted to enable direct comparability) via the closed-dynamic chamber method. Numeric values for soil CO<sub>2</sub> flux, soil temperature, and volumetric soil water content (VSWC) are the mean and standard deviation of field measurements at each site.

Site	Flux μmol m <sup>-2</sup> s <sup>-1</sup>	Soil temp °C	VSWC cm <sup>3</sup> cm <sup>-3</sup>	n
UNDE	2.55 ± 0.26	14.33 ± 0.77	0.33 ± 0.02	61
WOOD	3.02 ± 0.4	16.01 ± 1.54	0.28 ± 0.01	53
WREF	3.62 ± 0.3	15.34 ± 1.76	0.27 ± 0.06	21
KONZ	6.35 ± 0.97	27.28 ± 4.14	0.37 ± 0.01	44
SJER	0.94 ± 0.02	41.68 ± 11.22	0.01 ± 0.01	32
SRER	0.72 ± 0.09	47.64 ± 7.46	0.04 ± 0.01	32

298 LI-COR instruments to a given soil flux calculation from `neonSoilFlux` for each site and flux  
 299 computation method and quantified the relationship statistically ( $R^2$ ). Finally, for a half-hourly  
 300 interval we also computed a *post hoc* diffusivity ( $D_a$ ) using the LI-COR flux along with the  
 301 CO<sub>2</sub> surface gradient reported by NEON using the measurement levels closest to the surface.

## 302 4 Results

### 303 4.1 Concordance between modelled and measured soil CO<sub>2</sub> flux

304 The sites we visited ranged substantially in both their annual average temperature and  
 305 precipitation as well as their biome type (Table 2). These differences also influenced the wide  
 306 range of observed flux rates across sites.

307 The timeseries of the measured fluxes from the LI-COR 6800 and 870/8250 were compared  
 308 to modeled soil fluxes from the `neonSoilFlux` R package (Figure 4). We also assessed year-  
 309 long estimated flux time series and compared those to field measurements made at each site  
 310 (Figure 5). Results are reported in local time. Where applicable, sites are displayed from left

311 to right by increasing soil temperature (Table 1). Positive values of the flux indicate that there  
 312 is a flux moving towards the surface. Overall, with the exception of SRER (discussed later) the  
 313 computed fluxes determined using a variety of plausible methods spanned the field-measured  
 314 fluxes, but the specific flux-gradient method that best approximated field measurements varied  
 315 by site.

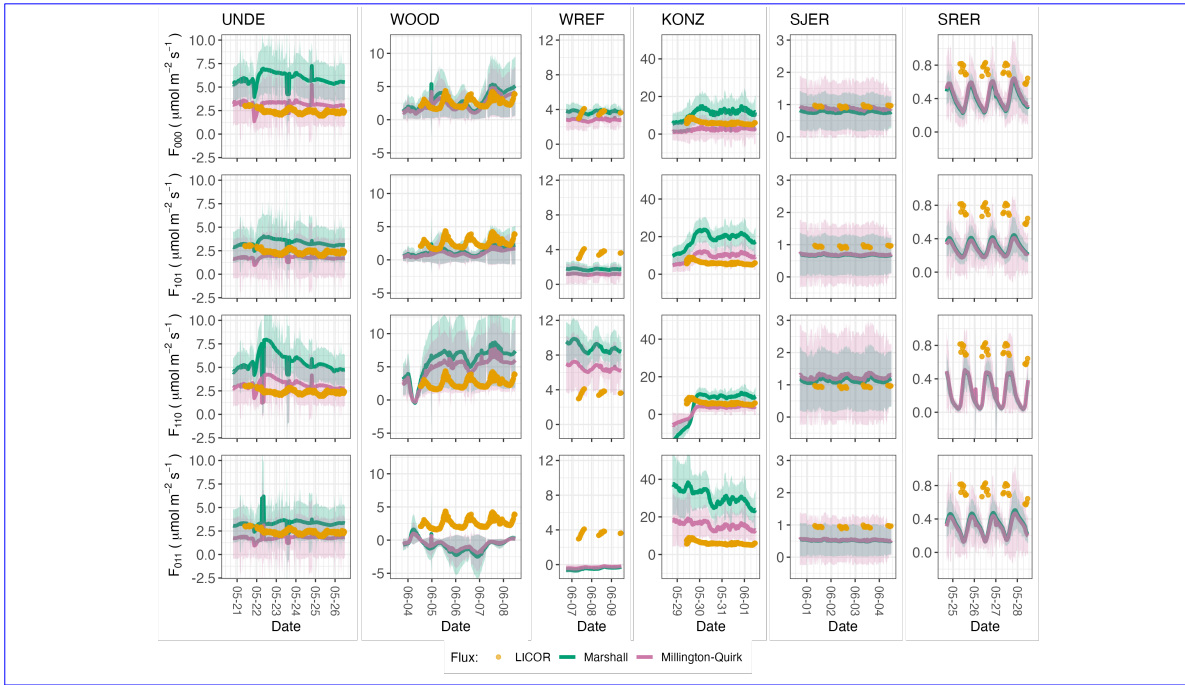


Figure 4: Timeseries of soil surface flux ( $F_S$ ) from field-measured (yellow lines) and modeled soil fluxes (green or purple lines) by the `neonSoilFlux` R package. Fluxes from the `neonSoilFlux` R package are separated by the diffusivity model used (Millington-Quirk or Marshall, Section 3.2.2). Individual vertical axis labels in the first column represent the measurement levels where the flux-gradient approach is applied (Section 3.2.3). Ribbons for modeled soil fluxes represent approximately  $\pm 1$  standard deviation. Results are reported in local time. WREF, SJER, and SRER were sampled in 2022, and UNDE, WOOD, and KONZ were sampled in 2024. Sites (columns) are arranged from left to right in terms of increasing mean annual temperature.

316 We calculated a statistical relationship between the various estimates of soil flux computed by  
 317 `neonSoilFlux` and the field-measured fluxes within daily interval periods. Statistics for these  
 318 comparisons are reported in Figure 6, which also shows how these fall relative to a 1:1 line.

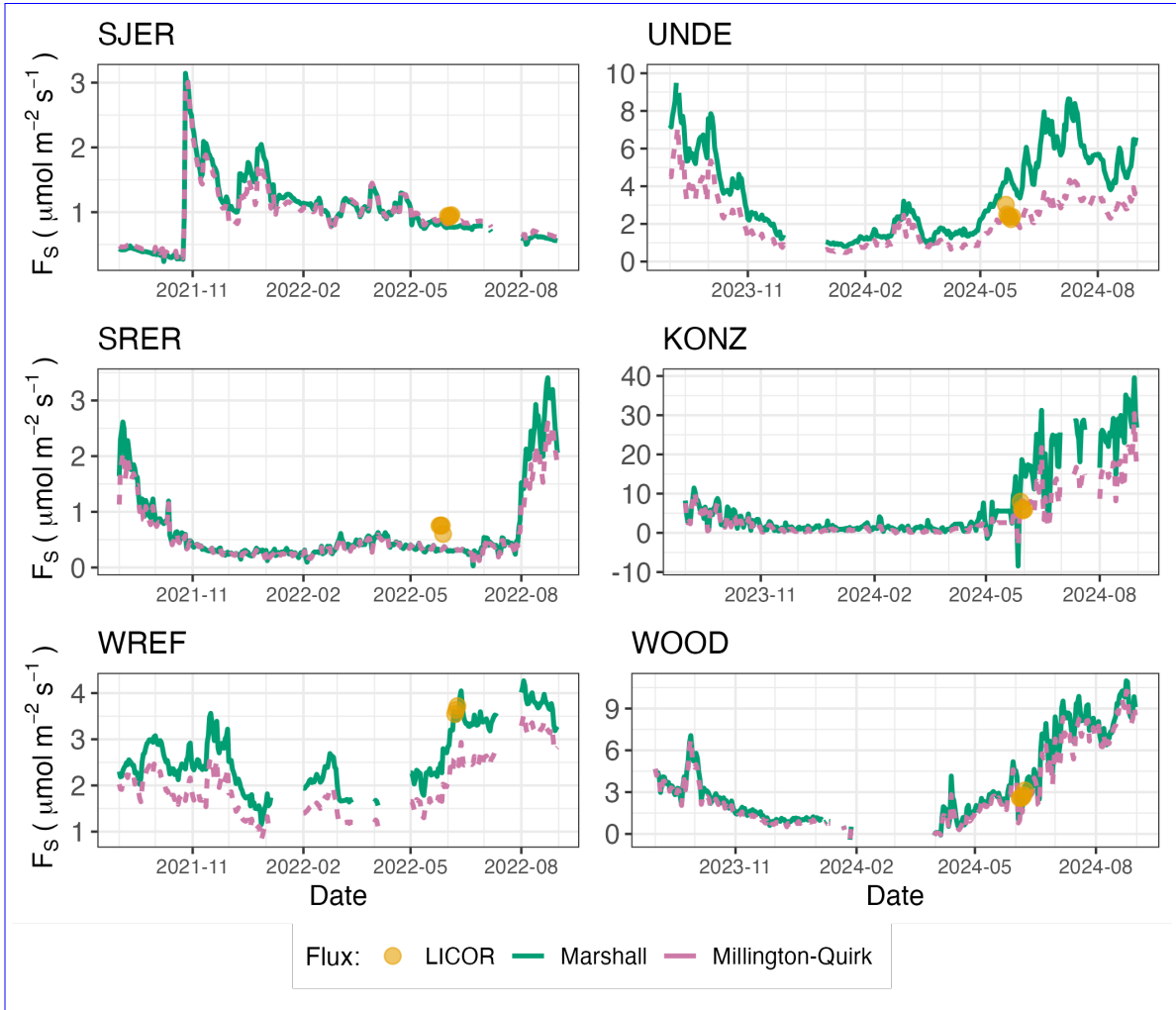


Figure 5: Timeseries of both daily-averaged field  $F_S$  (yellow circles) and daily ensemble averaged soil fluxes (average of  $F_{000}$ ,  $F_{101}$ ,  $F_{011}$ ,  $F_{110}$ , Section 3.2.3) by the `neonSoilFlux` R package, separated by the diffusivity model used (green or purple lines, Millington-Quirk or Marshall, Section 3.2.2).

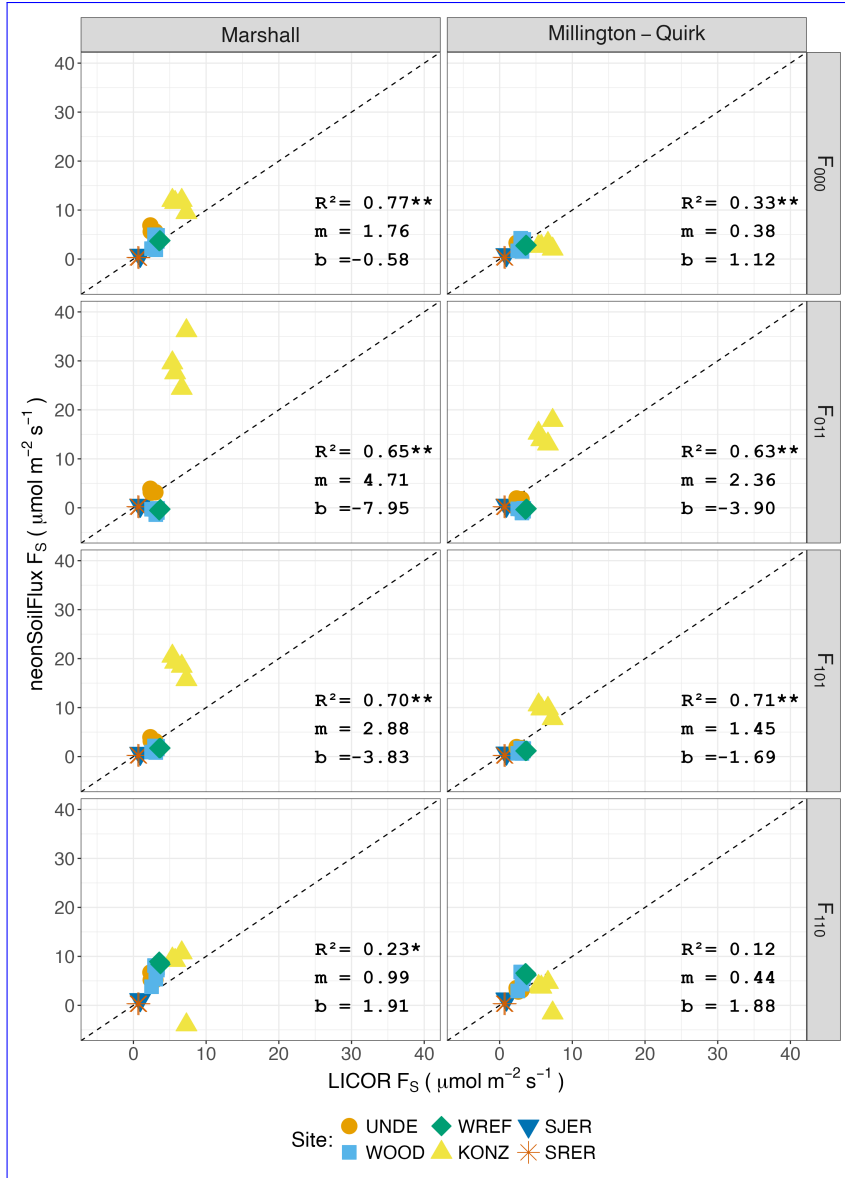


Figure 6: Statistical comparison between measured fluxes at each NEON site with fluxes reported by `neonSoilFlux` with the different flux calculation approaches and diffusivity calculations applied. Points are daily averages and LICOR  $F_S$  values are from the 6800 instrument only, for consistency. The dotted line represents a 1:1 relationship, and the reported  $R^2$  quantifies the relationship between field-measured and `neonSoilFlux` estimated fluxes. \* = significance at the 5% level, \*\* = significance at the 1% level. The slope (m) and intercept (b) of the linear regression between measured and modeled fluxes are also reported. The low-value outlier from KONZ in the  $F_{110}$  Marshall plot is an example of the effect of inverted CO<sub>2</sub> gradients causing an estimated flux to be negative, bringing down the daily mean, which later resolved as the soils dried back out.

319 **4.2 Effects of method choice on diffusivity estimates**

320 In ~~four of one of the~~ six field sites, the *post hoc*  $D_a$  estimate fell roughly between the two  
321 diffusion estimation methods; ~~however this was less the case in the two driest sites, SJER and~~  
322 ~~At UNDE, WOOD, WREF, and SJER, the median field estimate of diffusivity was lower~~  
323 ~~than both of the other methods. At the driest site, SRER (Table 1), where the the median~~  
324 field estimate of diffusivity was ~~either lower or~~ higher than both of the other methods and  
325 values showed a large amount of variation (Figure 7).

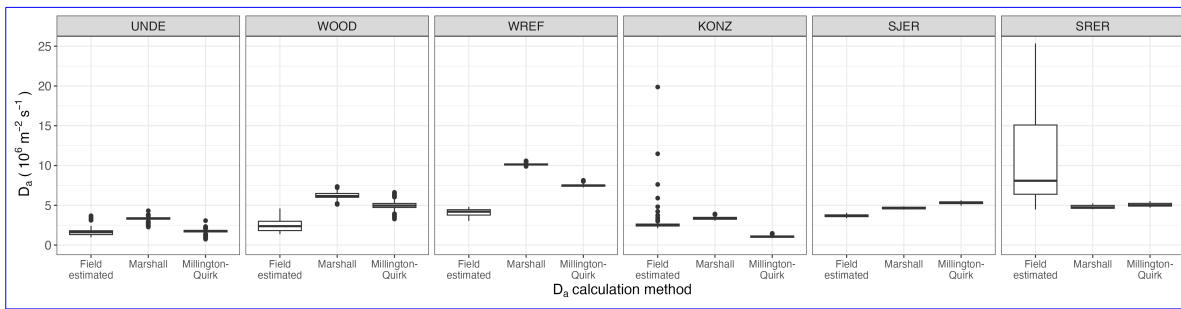


Figure 7: Distribution of diffusivity ( $D_a$ ) at each study site. Values of  $D_a$  were provided by the neonSoilFlux package, computed from the Millington-Quirk or Marshall models (Section 3.2.2). A post-hoc estimate of diffusivity (labeled as “Field estimated”) was computed through the field measured flux (Figure 4), divided by the CO<sub>2</sub> gradient from the measurement levels closest to the soil surface, as reported by NEON. We only used  $F_S$  measured by the LICOR 6800 at all sites to standardize comparisons. Some outliers ( $n = 1$  from the field estimated values at KONZ and  $n = 6$  from field estimated values at SRER) are excluded from the plot to allow better comparative visualization across sites.

326 **5 Discussion**

327 This study presents a unified data science workflow to efficiently process automated measure-  
328 ments of belowground soil CO<sub>2</sub> concentrations, soil water content, and soil temperature to  
329 infer estimates of soil surface CO<sub>2</sub> effluxes through application of Fick’s Law (Equation 4).

330 Our core goals in this study were: (1) to generate estimates of soil flux from continuous soil  
331 sensor data at terrestrial NEON sites using the flux-gradient method and then (2) to compare  
332 those estimates to field-measured fluxes based on the closed chamber approach at six NEON  
333 focal sites. We discuss our progress toward these core goals through (1) an overall evaluation  
334 of the flux-gradient approach (and uncertainty calculation) and (2) site-specific evaluation of  
335 differences in estimated vs measured fluxes.

336 **5.1 General evaluation of flux-gradient approach**

337 Key assumptions of the flux-gradient approach are that CO<sub>2</sub> concentrations increase throughout  
338 the soil profile such that the highest concentrations are observed in the deepest layers. Addition-  
339 ally, field flux measurements should correlate with  $F_{000}$  because they represent surface fluxes.  
340 Periods where this gradient condition are not met generally are connected to processes that occur  
341 during soil wetting events, where more shallow soil layers produce higher concentrations of CO<sub>2</sub>  
342 due to microbial respiration pulses following rewetting. This effect is likely to be largest at sites  
343 with rich organic soils (e.g. KONZ). Based on this reasoning, in these types of situations we would  
344 *a priori* expect  $F_{011}$  (deepest layers)  $\leq F_{101} \leq F_{110}$  (shallow layers)  $\leq F_{000}$  (all layers) be-  
345 cause the previous flux estimates rely primarily on CO<sub>2</sub> concentrations at deeper depths, and  
346 could miss high concentrations of CO<sub>2</sub> produced in shallower layers.

347 When modeling soil respiration, typically a non-linear response function that also considers soil  
348 type is used (Bouma & Bryla, 2000; Yan et al., 2016, 2018). For the `neonSoilFlux` package,  
349 soil type is connected to the measurement of bulk density, which was characterized at each  
350 NEON site. This bulk density estimate is based on replicate samples collected from the site  
351 megapit at a subset of soil horizons, with an estimated uncertainty of  $\pm 5\%$  ([National Ecological  
352 Observatory Network \(NEON\)](#)[NEON](#), 2024c). Coarse fragment estimates also have very large

353   uncertainties, but because the volume fraction tends to be low in surface soils it is unlikely to  
354   contribute much additional flux uncertainty.

355   Our results suggest that the most important way to improve reliability of the flux estimate is  
356   to reduce the usage of gap-filled data. The current approach to gap filling in `neonSoilFlux`  
357   uses monthly mean data to gap fill—this approach decreases the ability of the estimate to be  
358   responsive to short-term pulses that occur with rapid weather shifts. ~~Four sites (KONZ, SRER,  
359   WREF, and UNDE)~~ All sites had more than 75% of half-hourly periods with no-gap filled  
360   measurements (Figure S1, Supplementary Information). ~~Two sites (SJER and WOOD) had  
361   more than 75% of half hourly intervals with just one~~ At five out of six sites (all except SRER),  
362   we used at least some gap-filled measurement. ~~The large uncertainty evident in Figure 4 for  
363   estimates from WOOD and SJER are thus due in part to the gap filling used in these sites  
364   (Figure S1).~~ ~~While we did not need to use gap-filled measurements to compute the flux at  
365   of Soil Water Content (SWC).~~ At WREF, field data collection occurred following a severe  
366   rainstorm, with soils at the beginning of the sampling week near their water holding capacity,  
367   which can influence the soil moisture sensor accuracy. In general, we recommend that whenever  
368   possible, knowledge of local field conditions should influence analysis decisions in addition to  
369   any QA filtering protocols in the `neonSoilFlux` package.

370   We recognize that this gap-filling approach may lead to gap-filled values that are quite different  
371   from the actual values, such as an underestimate of soil moisture following rain events. Further  
372   extensions of the gap filling method could use more sophisticated gap-filling routines, similar to  
373   what is used for net ecosystem carbon exchange (Falge et al., 2001; Liu et al., 2023; Mariethoz  
374   et al., 2015; Moffat et al., 2007; Zhang et al., 2023). Additionally, since the deepest temperature  
375   and soil moisture sensors are located below the deepest CO<sub>2</sub> sensors at NEON sites, it is  
376   possible that excluding these deeper layers from consideration prior to analysis would lead to a  
377   reduced need for gap filling. Future iterations of the `neonSoilFlux` package may incorporate

378 this as an option. The current gap-filling routine provides a consistent approach that can be  
379 applied to each data stream, but further work may explore alternative gap-filling approaches.

## 380 **5.2 Evaluation of flux-gradient approach at each site**

381 Derived results from the `neonSoilFlux` package have patterns that are broadly consistent with  
382 those directly measured in the field (Figure 4 and Figure 5), even though statistical comparisons  
383 between the field-measured and `neonSoilFlux` values were quite variable (e.g.  $R^2$  ranging  
384 from ~~0.04 to 0.81~~0.12 to 0.77; Figure 6). One advantage of the `neonSoilFlux` package is its  
385 ability to calculate fluxes across different soil depths (Figure 3), which allows for additional  
386 site-specific customization. We believe the package can provide a useful baseline estimate of  
387 soil fluxes that can always be complemented through additional field measurements.

388 The six locations studied provide a range of case studies that suggest different considerations  
389 may apply to different sites when applying the flux-gradient method. For example, the Santa  
390 Rita Experimental Range (SRER) is a desert site characterized by sandy soil, which also was  
391 the location of the highest field soil temperatures that we observed (Table 2). At SRER the  
392 flux across the top two layers ( $F_{110}$ ) produced a pattern of soil flux most consistent with the  
393 observed field data. The remaining methods  $F_{101}$ ,  $F_{011}$ , or  $F_{000}$  are derived from information  
394 taken from the deepest layer, which seems to have been decoupled from the surface layers both  
395 in terms of temperature and CO<sub>2</sub> concentration. This may be a general circumstance where  
396 there are large diurnal temperature extremes that rapidly change during the course of a day  
397 and overnight, leading to lags in the timing of when temperature increases propagate down to  
398 deeper soil layers.

399 Immediately prior to our visit to Konza Prairie (KONZ), that site that experienced a significant  
400 rain event that led to wet soils that gradually dried out over the course of our time there.

401 This pulse of precipitation increased the soil CO<sub>2</sub> concentration at the top layer above the  
402 concentrations in lower layers, leading to negative estimated flux values at the start of the field  
403 sampling period. In this case it was only when the soil began to return to a baseline level that  
404 the assumptions of the flux-gradient method were again met.

405 Both of the previous cases also provide context for the variable statistical comparisons between  
406 field-measured soil fluxes and `neonSoilFlux` outputs (Figure 6). When considering systematic  
407 deployment of this method across a measurement network, there are a number of independent  
408 challenges that require careful consideration. There are clear tradeoffs between (1) accuracy of  
409 modeled fluxes (defined here as closeness to field-measured  $F_S$  and the uncertainty reduction  
410 factor  $\epsilon$ ), (2) precision (which could be defined by the signal to noise ratio), and (3) the choice of  
411 the diffusivity model (Section 3.2.2) or flux computation method (Section 3.2.3). ~~A sensitivity~~  
412 ~~analysis~~ We performed a sensitivity analysis to compare the impact of these factors (Figure S2,  
413 Supplemental Information) ~~found that flux output uncertainty was dominated by measurement~~  
414 ~~uncertainty ( $T_S$ ,  $P$ , SWC, or CO<sub>2</sub>) rather than by the diffusivity method used to compute soil~~  
415 ~~flux. Notably, the  $F_{110}$  method was least sensitive to measurement uncertainty likely because~~  
416 ~~it best aligns with the surface chamber measurement assumptions.~~ ~

417 Finally, comparing the effects of different diffusivity estimation methods on the match between  
418 modeled and measured fluxes (Figure 5) highlights the sensitivity of  $F_{ijk}$  to diffusivity. The  
419 comparison between diffusivity estimates compared to field estimated diffusivity (Figure 7)  
420 demonstrates that site parameters can dictate which measure of diffusivity is most likely to be  
421 accurate in a given environmental context. Site-specific differences are largely a reflection of  
422 differences in soil moisture across the sites (Table 1), as not all diffusivity estimation methods  
423 incorporate soil moisture equivalently. While we here have compares two approaches to calculate  
424 diffusivity (the Millington-Quirk and Marshall models), it may be valuable to evaluate other  
425 diffusivity models (e.g. the Moldrup model; Moldrup et al. (1999)) as well. Ultimately the

426 choice of a particular diffusivity model could be determined based on knowledge of site-specific  
427 evaluations or a set of these models could be used to generate a model ensemble average as a  
428 means to trade precision for a more general approach.

429 **5.3 Recommendations for future method development**

430 The `neonSoilFlux` package provides several approaches to estimate soil flux using the gradient  
431 method. We believe these approaches enable the software to be used across a range of site-  
432 specific assumptions (Maier & Schack-Kirchner, 2014). We note, however, that this choice  
433 can have a determinative approach on the calculated values. Ensemble averaging approaches  
434 (Elshall et al., 2018; Raftery et al., 2005) may be one way to address this problem if the goal  
435 is to calculate fluxes using the same method at a diverse range of different sites. Two other  
436 ideas would be to apply machine learning algorithms (~~e.g.~~ [e.g.](#) random forest) to generate a  
437 single flux estimate across diverse sites, or using co-located estimates of net ecosystem carbon  
438 exchange from eddy-flux towers to further constrain results or to assess soil flux results for  
439 plausibility (Phillips et al., 2017).

440 These challenges notwithstanding, the method used here and made available in the  
441 `neonSoilFlux` R package has the potential to produce nearly continuous estimates of flux  
442 across all terrestrial NEON sites. These estimates are a significant improvement on available  
443 approaches to constrain the portion of ecosystem respiration attributable to the soil. This, in  
444 turn, also aids in our ability to understand the soil contribution to the net ecosystem flux  
445 measured at these sites using the co-located eddy flux towers.

<sup>446</sup> **6 Conclusions**

<sup>447</sup> We used the R package `neonSoilFlux` to estimate soil CO<sub>2</sub> fluxes with the flux-gradient method  
<sup>448</sup> using data from buried soil sensors at NEON terrestrial sites. We compared the predicted  
<sup>449</sup> fluxes to those measured directly using a field-based closed chamber approach. Soil fluxes  
<sup>450</sup> from `neonSoilFlux` were broadly effective at producing estimates of flux comparable to those  
<sup>451</sup> measured in the field using a chamber-based technique. However `neonSoilFlux` outputs are  
<sup>452</sup> quite sensitive to a number of issues, including: missing data (and thus gap-filling of input  
<sup>453</sup> measurement datasets), the selection of soil depths used to best calculate the gradient (which  
<sup>454</sup> may vary between sites), and finally the choice of method used for estimating soil diffusivity.  
<sup>455</sup> The flexibility of the `neonSoilFlux` package allows the user to evaluate each of these issues  
<sup>456</sup> with site-specific knowledge and contexts. Future refinements and subsequent validation of  
<sup>457</sup> `neonSoilFlux` outputs will feed forward into evaluating soil carbon fluxes broader spatial scales  
<sup>458</sup> to enhance understanding of the ways in which soils across diverse ecosystems are responding  
<sup>459</sup> to a changing climate.

<sup>460</sup> **Sources Cited**

- <sup>461</sup> Ayres, E., Reichle, R. H., Colliander, A., Cosh, M. H., & Smith, L. (2024). Validation of  
<sup>462</sup> Remotely Sensed and Modeled Soil Moisture at Forested and Unforested NEON Sites.  
<sup>463</sup> *IEEE Journal of Selected Topics in Applied Earth Observations and Remote Sensing*, 17,  
<sup>464</sup> 14248–14264. <https://doi.org/10.1109/JSTARS.2024.3430928>
- <sup>465</sup> Baldocchi, D. (2014). Measuring fluxes of trace gases and energy between ecosystems and the  
<sup>466</sup> atmosphere - the state and future of the eddy covariance method. *Global Change Biology*,  
<sup>467</sup> 20(12), 3600–3609. <https://doi.org/10.1111/gcb.12649>

- 468 Berenbaum, M. R., Carpenter, S. R., Hampton, S. E., Running, S. W., & Stanzione, D. C.  
469 (2015). *Report from the NSF BIO Advisory Committee Subcommittee on NEON Scope*  
470 *Impacts*.
- 471 Bond-Lamberty, B. (2018). New Techniques and Data for Understanding the Global Soil  
472 Respiration Flux. *Earth's Future*, 6(9), 1176–1180. <https://doi.org/10.1029/2018EF000866>
- 473 Bond-Lamberty, B., Ballantyne, A., Berryman, E., Fluet-Chouinard, E., Jian, J., Morris, K.  
474 A., Rey, A., & Vargas, R. (2024). Twenty Years of Progress, Challenges, and Opportuni-  
475 ties in Measuring and Understanding Soil Respiration. *Journal of Geophysical Research: Bio-geosciences*, 129(2), e2023JG007637. <https://doi.org/10.1029/2023JG007637>
- 476 Bond-Lamberty, B., Christianson, D. S., Malhotra, A., Pennington, S. C., Sihi, D., AghaK-  
477 ouchak, A., Anjileli, H., Altaf Arain, M., Armesto, J. J., Ashraf, S., Ataka, M., Baldocchi,  
478 D., Andrew Black, T., Buchmann, N., Carbone, M. S., Chang, S.-C., Crill, P., Curtis, P.  
479 S., Davidson, E. A., ... Zou, J. (2020). COSORE: A community database for continuous  
480 soil respiration and other soil-atmosphere greenhouse gas flux data. *Global Change Biology*,  
481 26(12), 7268–7283. <https://doi.org/10.1111/gcb.15353>
- 482 Bond-Lamberty, B., & Thomson, A. (2010). A global database of soil respiration data.  
483 *Biogeosciences*, 7(6), 1915–1926. <https://doi.org/10.5194/bg-7-1915-2010>
- 484 Bond-Lamberty, B., Wang, C., & Gower, S. T. (2004). A global relationship between the  
485 heterotrophic and autotrophic components of soil respiration? *Global Change Biology*,  
486 10(10), 1756–1766. <https://doi.org/10.1111/j.1365-2486.2004.00816.x>
- 487 Bouma, T. J., & Bryla, D. R. (2000). On the assessment of root and soil respiration for soils of  
488 different textures: Interactions with soil moisture contents and soil CO<sub>2</sub> concentrations.  
489 *Plant and Soil*, 227(1), 215–221. <https://doi.org/10.1023/A:1026502414977>
- 490 Chen, H., & Tian, H.-Q. (2005). Does a General Temperature-Dependent Q10 Model of Soil  
491 Respiration Exist at Biome and Global Scale? *Journal of Integrative Plant Biology*, 47(11),  
492 1288–1302. <https://doi.org/10.1111/j.1744-7909.2005.00211.x>

- 494 Davidson, E. A., Janssens, I. A., & Luo, Y. (2006). On the variability of respiration in  
495 terrestrial ecosystems: Moving beyond Q10. *Global Change Biology*, 12, 154–164. <https://doi.org/10.1111/j.1365-2486.2005.01065.x>
- 496
- 497 Desai, A. R., Murphy, B. A., Wiesner, S., Thom, J., Butterworth, B. J., Koupaei-Abyazani, N.,  
498 Muttaqin, A., Paleri, S., Talib, A., Turner, J., Mineau, J., Merrelli, A., Stoy, P., & Davis,  
499 K. (2022). Drivers of Decadal Carbon Fluxes Across Temperate Ecosystems. *Journal of*  
500 *Geophysical Research: Biogeosciences*, 127(12), e2022JG007014. <https://doi.org/10.1029/2022JG007014>
- 501
- 502 Efron, B., & Tibshirani, R. J. (1994). *An Introduction to the Bootstrap*. Chapman and  
503 Hall/CRC. <https://doi.org/10.1201/9780429246593>
- 504 Elshall, A. S., Ye, M., Pei, Y., Zhang, F., Niu, G.-Y., & Barron-Gafford, G. A. (2018). Relative  
505 model score: A scoring rule for evaluating ensemble simulations with application to microbial  
506 soil respiration modeling. *Stochastic Environmental Research and Risk Assessment*, 32(10),  
507 2809–2819. <https://doi.org/10.1007/s00477-018-1592-3>
- 508 Falge, E., Baldocchi, D., Olson, R., Anthoni, P., Aubinet, M., Bernhofer, C., Burba, G.,  
509 Ceulemans, R., Clement, R., Dolman, H., Granier, A., Gross, P., Grünwald, T., Hollinger,  
510 D., Jensen, N.-O., Katul, G., Keronen, P., Kowalski, A., Lai, C. T., ... Wofsy, S. (2001).  
511 Gap filling strategies for defensible annual sums of net ecosystem exchange. *Agricultural  
512 and Forest Meteorology*, 107(1), 43–69. [https://doi.org/10.1016/S0168-1923\(00\)00225-2](https://doi.org/10.1016/S0168-1923(00)00225-2)
- 513 Farrance, I., & Frenkel, R. (2012). Uncertainty of Measurement: A Review of the Rules  
514 for Calculating Uncertainty Components through Functional Relationships. *The Clinical  
515 Biochemist Reviews*, 33(2), 49–75.
- 516 Friedlingstein, P., O’Sullivan, M., Jones, M. W., Andrew, R. M., Hauck, J., Landschützer,  
517 P., Le Quéré, C., Li, H., Luijkx, I. T., Olsen, A., Peters, G. P., Peters, W., Pongratz, J.,  
518 Schwingshackl, C., Sitch, S., Canadell, J. G., Ciais, P., Jackson, R. B., Alin, S. R., ...  
519 Zeng, J. (2025). Global Carbon Budget 2024. *Earth System Science Data*, 17(3), 965–1039.

- 520           <https://doi.org/10.5194/essd-17-965-2025>
- 521   Hamdi, S., Moyano, F., Sall, S., Bernoux, M., & Chevallier, T. (2013). Synthesis analysis  
522   of the temperature sensitivity of soil respiration from laboratory studies in relation to  
523   incubation methods and soil conditions. *Soil Biology and Biochemistry*, 58, 115–126.  
524           <https://doi.org/10.1016/j.soilbio.2012.11.012>
- 525   Jackson, R. B., Lajtha, K., Crow, S. E., Hugelius, G., Kramer, M. G., & Piñeiro, G. (2017).  
526   The Ecology of Soil Carbon: Pools, Vulnerabilities, and Biotic and Abiotic Controls.  
527   *Annual Review of Ecology, Evolution and Systematics*, 48(Volume 48, 2017), 419–445.  
528           <https://doi.org/10.1146/annurev-ecolsys-112414-054234>
- 529   Jian, J., Bailey, V., Dorheim, K., Konings, A. G., Hao, D., Shiklomanov, A. N., Snyder,  
530   A., Steele, M., Teramoto, M., Vargas, R., & Bond-Lamberty, B. (2022). Historically  
531   inconsistent productivity and respiration fluxes in the global terrestrial carbon cycle. *Nature  
532   Communications*, 13(1), 1733. <https://doi.org/10.1038/s41467-022-29391-5>
- 533   Jian, J., Vargas, R., Anderson-Teixeira, K., Stell, E., Herrmann, V., Horn, M., Kholod, N.,  
534   Manzon, J., Marchesi, R., Paredes, D., & Bond-Lamberty, B. (2021). A restructured and  
535   updated global soil respiration database (SRDB-V5). *Earth System Science Data*, 13(2),  
536   255–267. <https://doi.org/10.5194/essd-13-255-2021>
- 537   Jiang, J., Feng, L., Hu, J., Liu, H., Zhu, C., Chen, B., & Chen, T. (2024). Global soil  
538   respiration predictions with associated uncertainties from different spatio-temporal data  
539   subsets. *Ecological Informatics*, 82, 102777. <https://doi.org/10.1016/j.ecoinf.2024.102777>
- 540   Jobbágy, E. G., & Jackson, R. B. (2000). The Vertical Distribution of Soil Organic Carbon  
541   and its Relation to Climate and Vegetation. *Ecological Applications*, 10(2), 423–436.  
542           [https://doi.org/10.1890/1051-0761\(2000\)010%5B0423:TVDOSO%5D2.0.CO;2](https://doi.org/10.1890/1051-0761(2000)010%5B0423:TVDOSO%5D2.0.CO;2)
- 543   Jurasinski, G., Koebisch, F., Guenther, A., & Beetz, S. (2022). *Flux: Flux Rate Calculation  
544   from Dynamic Closed Chamber Measurements.*
- 545   Liu, K., Li, X., Wang, S., & Zhang, H. (2023). A robust gap-filling approach for European

- 546 Space Agency Climate Change Initiative (ESA CCI) soil moisture integrating satellite  
547 observations, model-driven knowledge, and spatiotemporal machine learning. *Hydrology*  
548 and *Earth System Sciences*, 27(2), 577–598. <https://doi.org/10.5194/hess-27-577-2023>
- 549 Lunch, C., Laney, C., Mietkiewicz, N., Sokol, E., Cawley, K., & NEON (National Ecological  
550 Observatory Network). (Network). N. (National. E. Q.). (2025). *neonUtilities: Utilities for*  
551 *working Working with NEON dataData*.
- 552 Luo, Y., Ogle, K., Tucker, C., Fei, S., Gao, C., LaDeau, S., Clark, J. S., & Schimel, D. S. (2011).  
553 Ecological forecasting and data assimilation in a data-rich era. *Ecological Applications*,  
554 21(5), 1429–1442. <https://doi.org/10.1890/09-1275.1>
- 555 Maier, M., & Schack-Kirchner, H. (2014). Using the gradient method to determine soil gas  
556 flux: A review. *Agricultural and Forest Meteorology*, 192–193, 78–95. <https://doi.org/10.1016/j.agrformet.2014.03.006>
- 558 Mariethoz, G., Linde, N., Jougnot, D., & Rezaee, H. (2015). Feature-preserving interpolation  
559 and filtering of environmental time series. *Environmental Modelling & Software*, 72, 71–76.  
560 <https://doi.org/10.1016/j.envsoft.2015.07.001>
- 561 Marshall, T. J. (1959). The Diffusion of Gases Through Porous Media. *Journal of Soil Science*,  
562 10(1), 79–82. <https://doi.org/10.1111/j.1365-2389.1959.tb00667.x>
- 563 Millington, R. J., & Shearer, R. C. (1971). Diffusion in aggregated porous media. *Soil Science*,  
564 111(6), 372–378.
- 565 Moffat, A. M., Papale, D., Reichstein, M., Hollinger, D. Y., Richardson, A. D., Barr, A. G.,  
566 Beckstein, C., Braswell, B. H., Churkina, G., Desai, A. R., Falge, E., Gove, J. H., Heimann,  
567 M., Hui, D., Jarvis, A. J., Kattge, J., Noormets, A., & Stauch, V. J. (2007). Comprehensive  
568 comparison of gap-filling techniques for eddy covariance net carbon fluxes. *Agricultural and*  
569 *Forest Meteorology*, 147(3), 209–232. <https://doi.org/10.1016/j.agrformet.2007.08.011>
- 570 Moldrup, P., Olesen, T., Yamaguchi, T., Schjønning, P., & Rolston, D. E. (1999). Modeling  
571 diffusion and reaction in soils: 9. The Buckingham-Burdine-Campbell equation for gas

- 572 diffusivity in undisturbed soil. *Soil Science*, 164(2), 75.
- 573 ~~National Ecological Observatory Network (NEON)~~NEON. (2024a). *Barometric pres-*  
574 *sure (DP1.00004.001)*. National Ecological Observatory Network (NEON). <https://doi.org/10.48443/RT4V-KZ04>
- 575 ~~National Ecological Observatory Network (NEON)~~NEON. (2024b). *Soil CO<sub>2</sub> concentration*  
576 *(DP1.00095.001)*. National Ecological Observatory Network (NEON). <https://doi.org/10.48443/E7GR-6G94>
- 577 ~~National Ecological Observatory Network (NEON)~~NEON. (2024c). *Soil physical and chemical*  
578 *properties, Megapit (DP1.00096.001)*. National Ecological Observatory Network (NEON).  
<https://doi.org/10.48443/S6ND-Q840>
- 579 ~~National Ecological Observatory Network (NEON)~~NEON. (2024d). *Soil tempera-*  
580 *ture (DP1.00041.001)*. National Ecological Observatory Network (NEON). <https://doi.org/10.48443/Q24X-PW21>
- 581 ~~National Ecological Observatory Network (NEON)~~NEON. (2024e). *Soil water content and*  
582 *water salinity (DP1.00094.001)*. National Ecological Observatory Network (NEON). <https://doi.org/10.48443/A8VY-Y813>
- 583 Norman, J. M., Kucharik, C. J., Gower, S. T., Baldocchi, D. D., Crill, P. M., Rayment,  
584 M., Savage, K., & Striegl, R. G. (1997). A comparison of six methods for measuring  
585 soil-surface carbon dioxide fluxes. *Journal of Geophysical Research: Atmospheres*, 102(D24),  
586 28771–28777. <https://doi.org/10.1029/97JD01440>
- 587 Pedersen, A. R. (2024). *HMR: Flux Estimation with Static Chamber Data*.
- 588 Phillips, C. L., Bond-Lamberty, B., Desai, A. R., Lavoie, M., Risk, D., Tang, J., Todd-Brown,  
589 K., & Vargas, R. (2017). The value of soil respiration measurements for interpreting and  
590 modeling terrestrial carbon cycling. *Plant and Soil*, 413(1), 1–25. <https://doi.org/10.1007/s11104-016-3084-x>
- 591 Raftery, A. E., Gneiting, T., Balabdaoui, F., & Polakowski, M. (2005). *Using Bayesian Model*
- 592
- 593
- 594
- 595
- 596

- 598      *Averaging to Calibrate Forecast Ensembles.* <https://doi.org/10.1175/MWR2906.1>
- 599      Rheault, K., Christiansen, J. R., & Larsen, K. S. (2024). goFlux: A user-friendly way to  
600      calculate GHG fluxes yourself, regardless of user experience. *Journal of Open Source  
601      Software*, 9(96), 6393. <https://doi.org/10.21105/joss.06393>
- 602      Sallam, A., Jury, W. A., & Letey, J. (1984). Measurement of Gas Diffusion Coefficient under  
603      Relatively Low Air-filled Porosity. *Soil Science Society of America Journal*, 48(1), 3–6.  
604      <https://doi.org/10.2136/sssaj1984.03615995004800010001x>
- 605      Shao, J., Zhou, X., Luo, Y., Li, B., Aurela, M., Billesbach, D., Blanken, P. D., Bracho, R.,  
606      Chen, J., Fischer, M., Fu, Y., Gu, L., Han, S., He, Y., Kolb, T., Li, Y., Nagy, Z., Niu, S.,  
607      Oechel, W. C., ... Zhang, J. (2015). Biotic and climatic controls on interannual variability  
608      in carbon fluxes across terrestrial ecosystems. *Agricultural and Forest Meteorology*, 205,  
609      11–22. <https://doi.org/10.1016/j.agrformet.2015.02.007>
- 610      Shao, P., Zeng, X., Moore, D. J. P., & Zeng, X. (2013). Soil microbial respiration from  
611      observations and Earth System Models. *Environmental Research Letters*, 8(3), 034034.  
612      <https://doi.org/10.1088/1748-9326/8/3/034034>
- 613      Sihi, D., Gerber, S., Inglett, P. W., & Inglett, K. S. (2016). Comparing models of microbial–  
614      substrate interactions and their response to warming. *Biogeosciences*, 13(6), 1733–1752.  
615      <https://doi.org/10.5194/bg-13-1733-2016>
- 616      Tang, J., Baldocchi, D. D., Qi, Y., & Xu, L. (2003). Assessing soil CO<sub>2</sub> efflux using continuous  
617      measurements of CO<sub>2</sub> profiles in soils with small solid-state sensors. *Agricultural and Forest  
618      Meteorology*, 118(3), 207–220. [https://doi.org/10.1016/S0168-1923\(03\)00112-6](https://doi.org/10.1016/S0168-1923(03)00112-6)
- 619      Tang, J., Misson, L., Gershenson, A., Cheng, W., & Goldstein, A. H. (2005). Continuous  
620      measurements of soil respiration with and without roots in a ponderosa pine plantation  
621      in the Sierra Nevada Mountains. *Agricultural and Forest Meteorology*, 132(3), 212–227.  
622      <https://doi.org/10.1016/j.agrformet.2005.07.011>
- 623      Taylor, J. R. (2022). *An Introduction to Error Analysis: The Study of Uncertainties in Physical*

- 624 *Measurements*, Third Edition (3rd ed.). University Science Press.
- 625 Wilson, S. J., Bond-Lamberty, B., Noyce, G., Bittencourt Peixoto, R., & Megonigal,  
626 J. P. (2024). Fluxfinder: An R Package for Reproducible Calculation and Initial  
627 Processing of Greenhouse Gas Fluxes From Static Chamber Measurements. *Journal of*  
628 *Geophysical Research: Biogeosciences*, 129(11), e2024JG008208. <https://doi.org/10.1029/2024JG008208>
- 630 Yan, Z., Bond-Lamberty, B., Todd-Brown, K. E., Bailey, V. L., Li, S., Liu, C., & Liu, C. (2018).  
631 A moisture function of soil heterotrophic respiration that incorporates microscale processes.  
632 *Nature Communications*, 9(1), 2562. <https://doi.org/10.1038/s41467-018-04971-6>
- 633 Yan, Z., Liu, C., Todd-Brown, K. E., Liu, Y., Bond-Lamberty, B., & Bailey, V. L. (2016).  
634 Pore-scale investigation on the response of heterotrophic respiration to moisture conditions  
635 in heterogeneous soils. *Biogeochemistry*, 131(1), 121–134. <https://doi.org/10.1007/s10533-016-0270-0>
- 637 Zhang, R., Kim, S., Kim, H., Fang, B., Sharma, A., & Lakshmi, V. (2023). Temporal Gap-Filling  
638 of 12-Hourly SMAP Soil Moisture Over the CONUS Using Water Balance Budgeting. *Water  
639 Resources Research*, 59(12), e2023WR034457. <https://doi.org/10.1029/2023WR034457>
- 640 Zhao, J. (2019). FluxCalR: A R package for calculating CO<sub>2</sub> and CH<sub>4</sub> fluxes from static  
641 chambers. *Journal of Open Source Software*, 4(43), 1751. <https://doi.org/10.21105/joss.01751>
- 643 Zobitz, J., Ayres, E., O'Rourke, K., Werbin, Z., Lee, L., Abdi, R., Mehmeti, D., & Xiong, L.  
644 (2024). *neonSoilFlux*: Compute Soil Carbon Fluxes for the National Ecological Observatory  
645 Network Sites.